tip with relatively high speed compared with one of branch elongation.

Supplemental Figure S4 -

Fig. S4. Identification of "cell-mixing" phenomenon during murine retinal angiogenesis in vivo. Murine retinal vasculature was immunostained with CD31 or CD34 at 6 and 12 hours after intravascular injection of BS-1 lectin. (A) Serial confocal images along the z-axis at 6 hours after the injection. Confocal images confirmed that lectin was labeled on the CD31+ ECs (arrowheads). (B) Z-stack confocal images of retinal vasculature 12 hours after the injection. Lectin-labeled ECs (arrowheads) were observed sporadically in the distal regions of CD34+ sprouts (B, part a). Conversely, in more proximal regions, lectin-unlabeled ECs (yellow asterisk indicates an example) were sporadically observed in lectin-labeled sprouts (B, part b). Arrows indicate the direction of vessel elongation. Scale bars: 25 μm.

Supplemental Figure S5 -

Fig. S5. Effects of Dll4-neutralizing and DAPT treatments on the morphology of sprouts in an in vitro angiogenesis. Murine aortic ring assay was performed in the absence (control) or presence of anti-Dll4-antibody (Ab) (A) or DAPT (B). Upper panel, iz-stack images of angiogenic sprouts positive for CD31 at day 7 of the culture. Lower panel, quantitative analyses of morphology changes. Anti-Dll4-Ab treatment increased branch point formation and total length of angiogenic sprouts (A). Similarly, DAPT treatment enhanced branch formation (B). Spouts were wider in DAPT treatment, although there was no change in the total length of angiogenic sprouts. Scale bars: 400 μm. Data are presented as mean±s.e.m. *P<0.05, **P<0.01. CTL indicates control.

Supplemental Figure S6 -

Fig. S6. Single- and multi-regression analysis between vessel elongation and the other parameters for collective EC movement. (A) Parameters at the tip and at the stalk and junction for collective EC movement driving vessel elongation. (B) Single regression analyses between vessel elongation and parameters for collective EC movement were performed. (C) Through the single regression analyses, seven out of 10 parameters for collective EC movement significantly correlated with vessel elongation, and then seven parameters were selected as explanatory variables for vessel elongation in following multi-regression analysis. B, β, and VIF indicate unstandardized coefficient, standardized coefficient and variance inflation factor, respectively.

Movie 1 -

Movie 1. Dynamic behavior of ECs during angiogenic sprouting in mouse aortic ring

assay. Images were taken every 15 minutes for 36 hours. (Left) Merged z-stack images of confocal and phase-contrast views. (Middle) Z-stack confocal images. (Right) Schematic images showing nuclear positions of individual ECs. ECs were clustered 5 to 10 in the same color to show mixing of ECs. Complex and heterogeneous EC movement during angiogenic sprouting was visualized. Some cells move backwards even though the branch is elongating and ECs from proximal ends (vascular bed) participate in forming branches.

Movie 2 -

Movie 2. Distinction between ECs and MCs in the angiogenic sprouts of wild-type (left) and EdnraEGFP (right) mice by nuclear stain with SYTO dyes. Images were taken at the interval of 5 minutes for 5 hours. Nuclei of ECs were strongly stained with SYTO dyes, whereas MC nuclei were only faintly stained. MCs can be identified by their morphology (left) and EGFP signals (right). Fourteen frames were taken every second.

Movie 3 -

Movie 3. Visualization of individual EC behavior in angiogenic sprouts by mosaic analysis. Images were taken every 7 minutes for 9 hours. (Left) Phase-contrast images. (Middle, right) Z-stack confocal images. See Materials and methods for mosaic analysis. An EGFP-labeled EC with lectin (red) (marked with red closed circle) overtakes a tip cell and is then replaced by a follower EC without EGFP signal (marked with yellow closed circles). In addition, a highly motile EC (marked with red circles) displays forward-rear cell polarity, whereas a low motile EC (white arrowhead) displays spindle shape without cell polarity. Blue indicates nuclear stain with SYTO dye. Fourteen frames were taken every second.

Movie 4 -

Movie 4. Visualization of the behavior of individual ECs in angiogenic sprouts by mosaic analysis. Images were taken every 5 minutes for 12 hours. (Left) Phase-contrast images. (Right) Z-stack confocal images. See Materials and methods for mosaic analysis. An EGFP-labeled EC at the tip starts to move in opposite direction against vessel elongation at a certain moment. The cell polarity dynamically changes depending on the moving direction. Blue indicates nuclear stain with SYTO dye. Fourteen frames were taken every second.

Movie 5 -

Movie 5. Visualization of the behavior of individual ECs in angiogenic sprouts by mosaic analysis. (Left) Phase-contrast images. (Right) Z-stack confocal images. See Materials and methods regarding mosaic analysis. An EC (white arrowhead) loses cell

polarity just before being taken over by a follower (red arrowhead); the EC gains cell polarity again at the next moment and starts to move to the tip (yellow arrowhead). Blue indicates nuclear stain with SYTO dye. Fourteen frames were taken every second.

Movie 6 -

Movie 6. Comparison of angiogenesis between different doses of VEGF. Images were taken every 15 minutes for 36 hours. Merged images of z-stack confocal and phase-contrast views. Nuclei were visualized by staining with SYTO dye (green). (Left) VEGF 0 ng/ml. (Right) VEGF 50 ng/ml. With higher VEGF, there is more branch elongation and sprouting out. ECs seem to move more rapidly. Fourteen frames were taken every second.

Movie 7 -

Movie 7. Comparison of angiogenesis between Dll4-Ab (right) and control IgG (left), both with VEGF 50 ng/ml. Images were taken every 15 minutes for 36 hours. Merged images of z-stack confocal and phase-contrast views. Nuclei were visualized by staining with SYTO dye (green). In the images, the nuclei of each EC are pseudocolored. There is excessive elongation in Dll4-Ab group. In addition, ECs seem to move faster as a whole than they do in control settings. Fourteen frames were taken every second.

Movie 8 -

Movie 8. Comparison of angiogenesis between DAPT (right) and control DMSO (left), both with VEGF 50 ng/ml. Images were taken every 15 minutes for 36 hours. (Upper panels) Z-stack confocal images. (Lower panels) Merged images of z-stack confocal and phase-contrast views. Nuclei were visualized by staining with SYTO dye (green). ECs move faster as a whole in the DAPT group than they do in control settings. In addition, more ECs seem to migrate backwards in the DPAT group when the branch is elongating forwards. Fourteen frames were taken every second.

Movie 9 -

Movie 9. Comparison of angiogenesis between PDFGRß-Ab (right) and control IgG (left), both with VEGF 50 ng/ml. This movie relates to Fig. 7. Images were taken every 15 minutes for 36 hours. (Upper panels) Z-stack confocal images. (Lower panels) Merged images of z-stack confocal and phase-contrast views. Nuclei were visualized by staining with SYTO dye (green). More ECs migrate backwards when the branch is elongated forwards in PDFGRß-Ab treatment than they do in control settings, resulting in retarded branch elongation. Fourteen frames were taken every second.

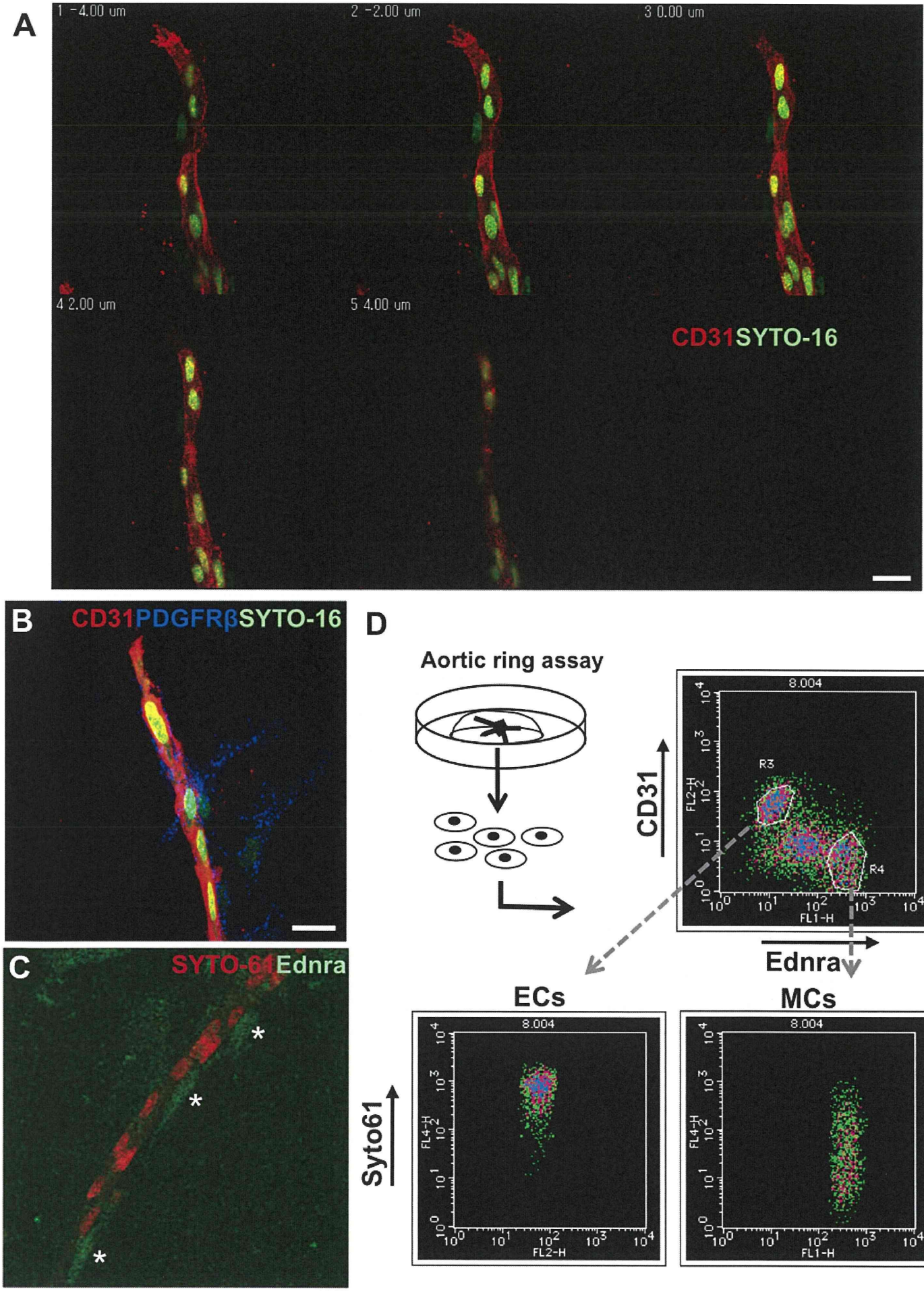
A
1 -4.00 um
2 -2.00 um
3 0.00 um
4 2.00 um
5 4.00 um
CD31SYTO-16
B
CD31PDGFRβSYTO-16
C
SYTO-61Ednra
D
Aortic ring assay
CD31
Ednra
8.004
R3
R4
FL2-H
FL1-H
ECs
MCs
Syto61
FL4-H

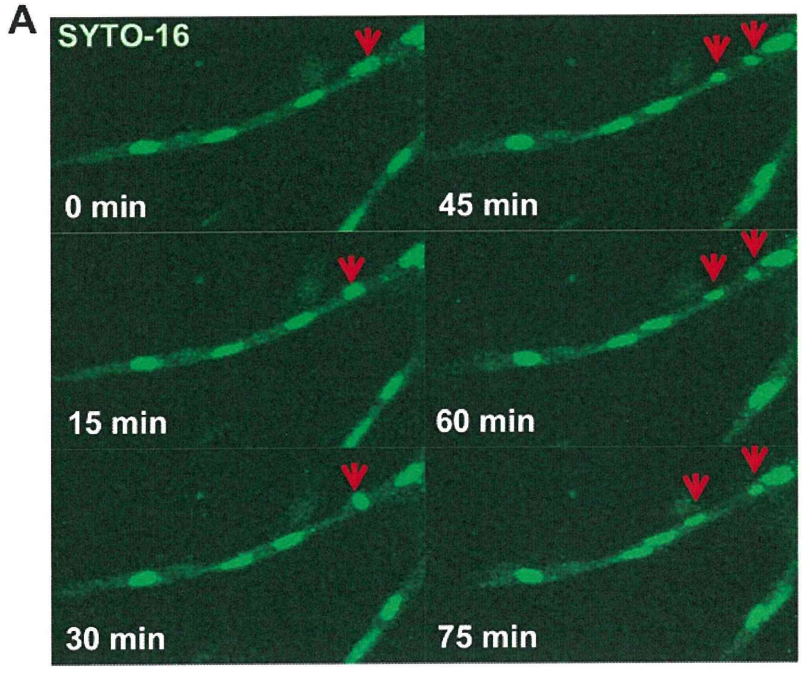
A
SYTO-16
0 min
45 min
15 min
60 min
30 min
75 min

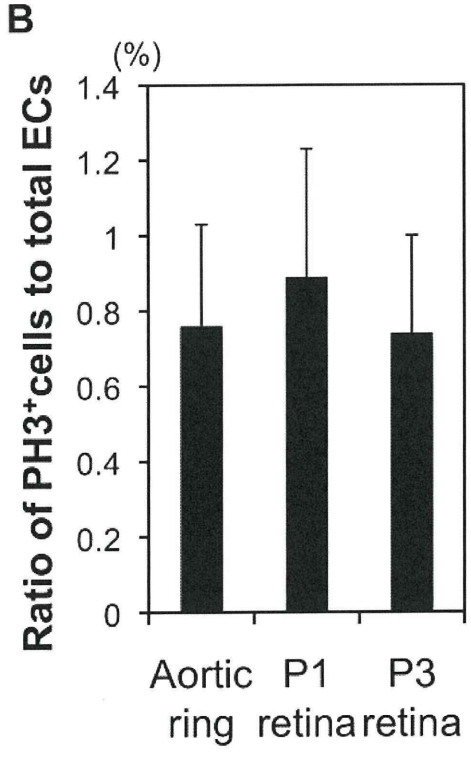
B
(%)
Ratio of PH3+cells to total ECs
1.4
1.2
1
0.8
0.6
0.4
0.2
0
Aortic ring
P1 retina
P3 retina

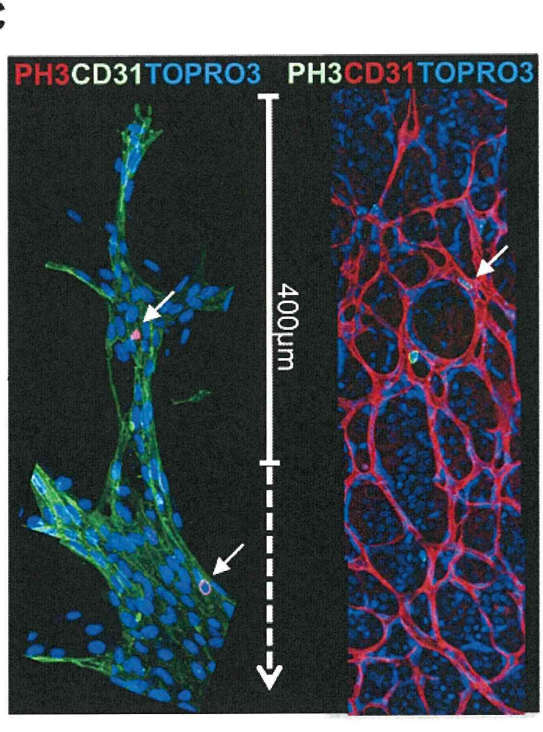
C
PH3CD31TOPRO3
PH3CD31TOPRO3
400μm

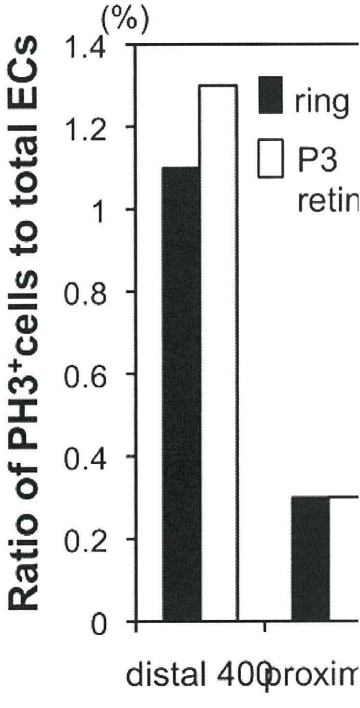
(%)
Ratio of PH3+cells to total ECs
1.4
1.2
1
0.8
0.6
0.4
0.2
0
ring
P3 retin
distal 400
proxim

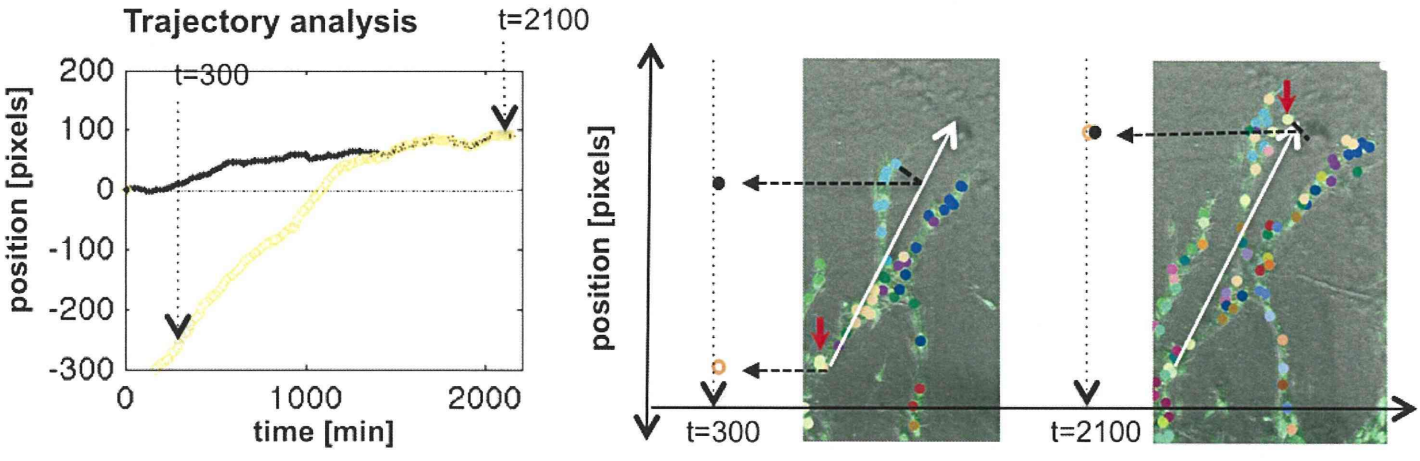
Trajectory analysis
t=2100
t=300
200
100
0
-100
-200
-300
position [pixels]
0
1000
2000
time [min]
position [pixels]
t=300
t=2100

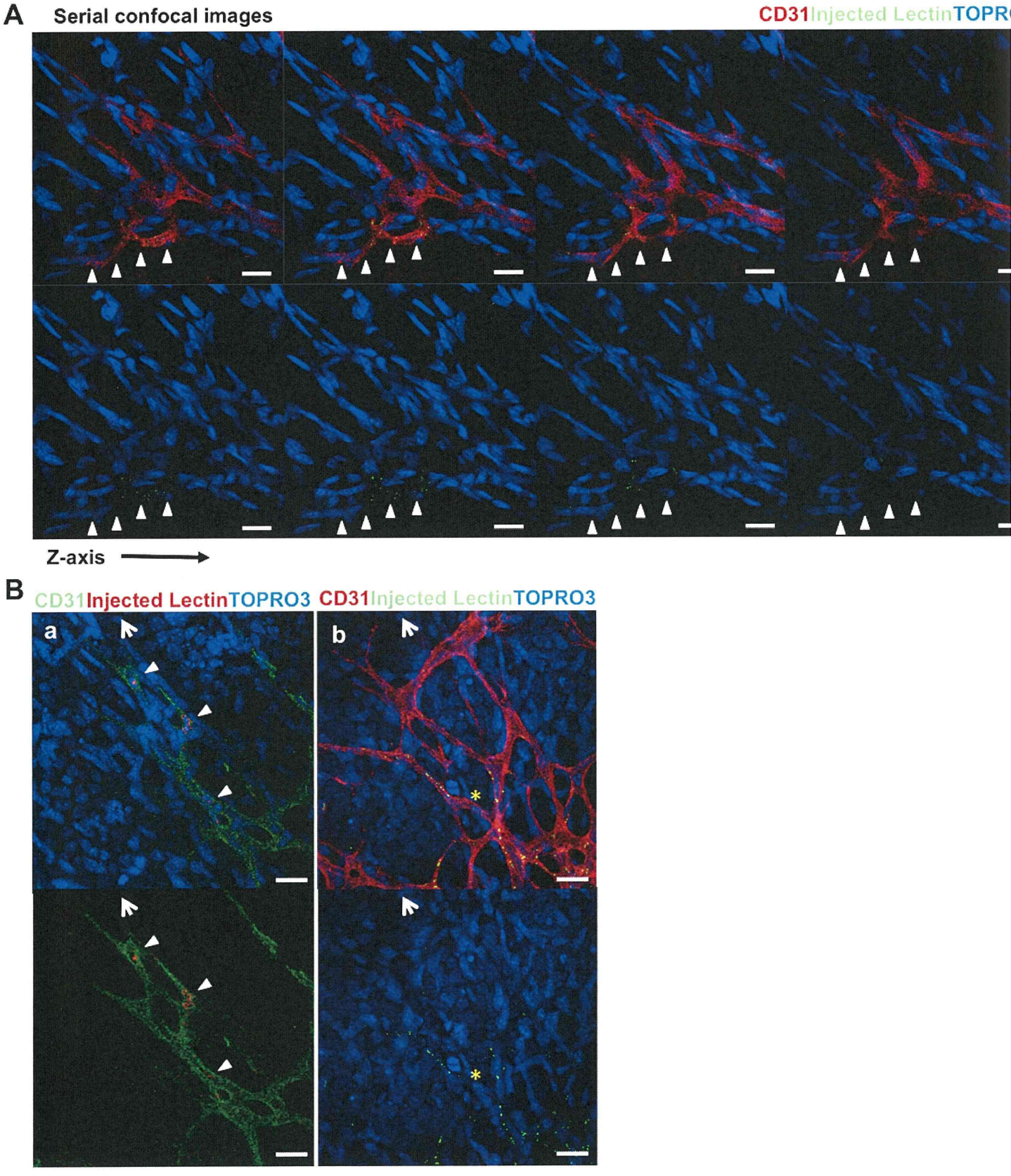
A
Serial confocal images
CD31Injected LectinTOPR
Z-axis
B
CD31Injected LectinTOPRO3
CD31Injected LectinTOPRO3
a
b

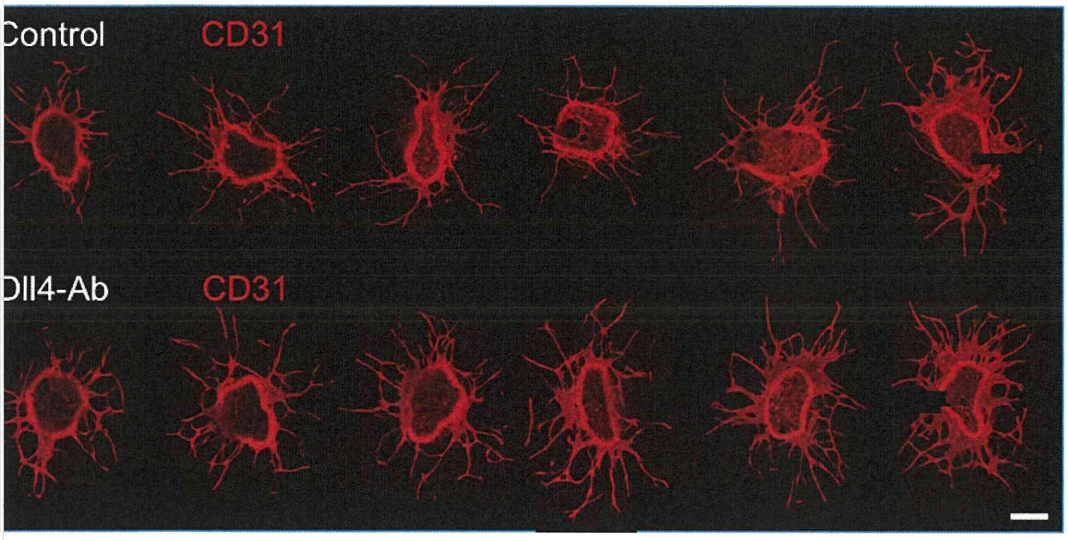
Control
CD31
Dll4-Ab
CD31

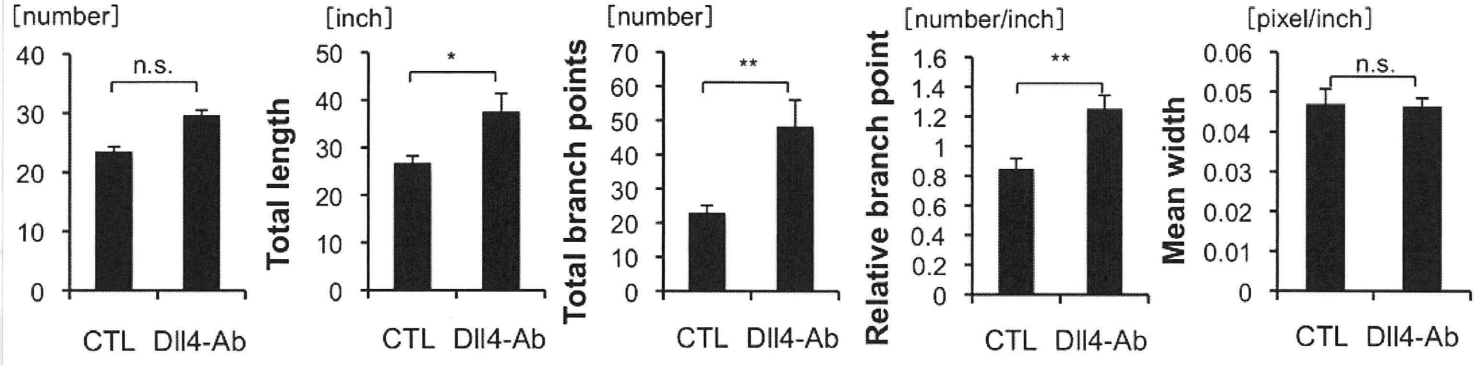
[number]
n.s.
CTL Dll4-Ab
[inch]
Total length
*
CTL Dll4-Ab
[number]
Total branch points
**
CTL Dll4-Ab
[number/inch]
Relative branch point
**
CTL Dll4-Ab
[pixel/inch]
Mean width
n.s.
CTL Dll4-Ab

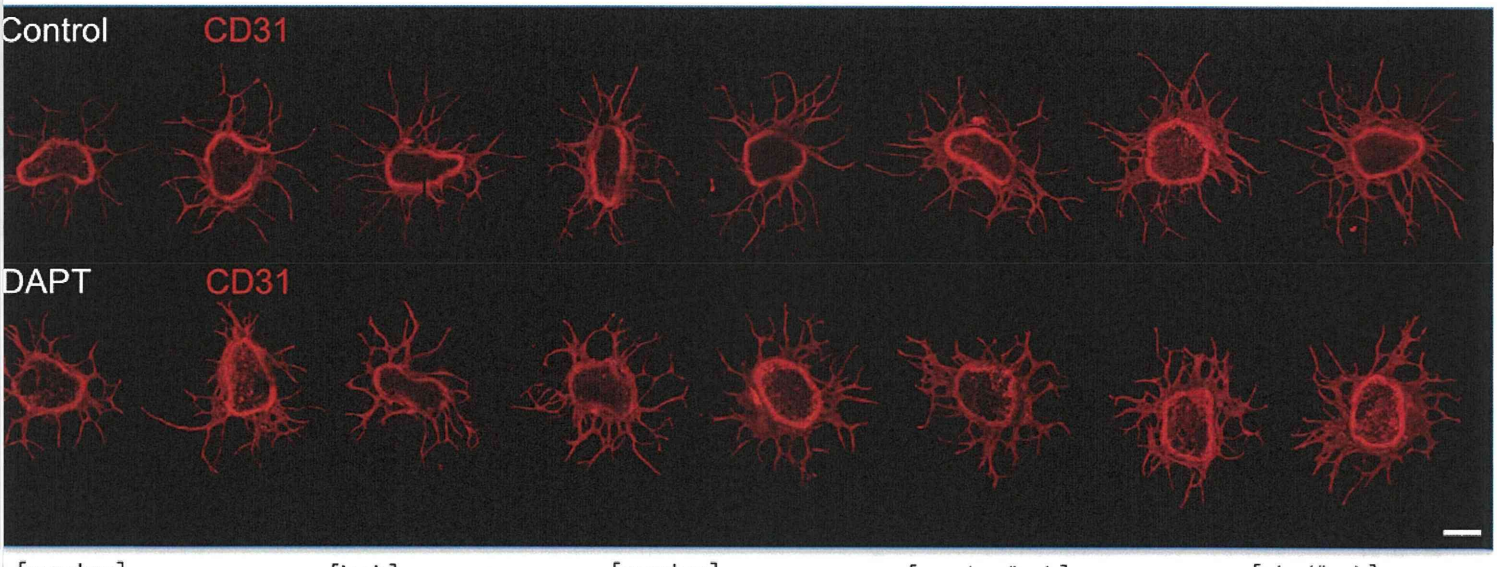
Control
CD31
DAPT
CD31

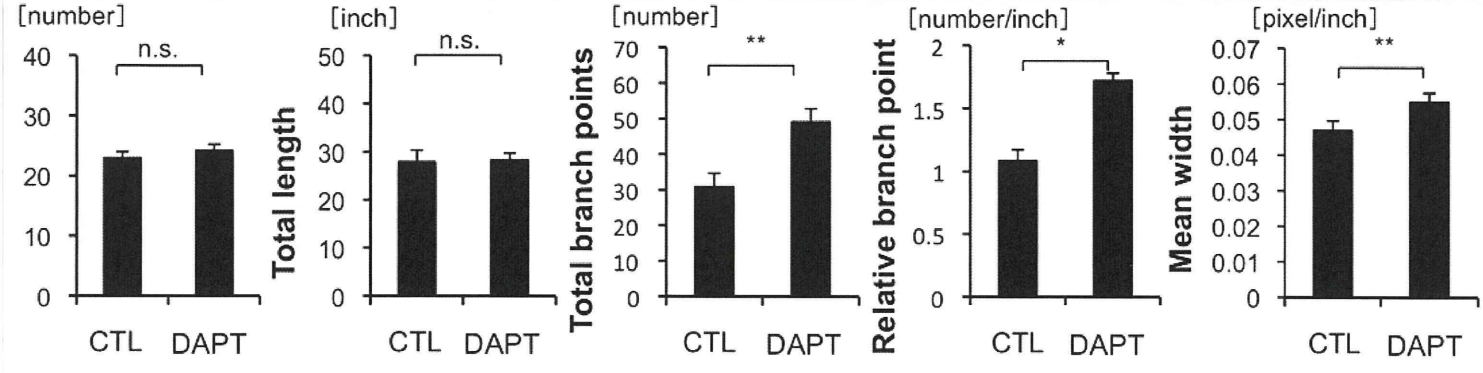
[number]
n.s.
CTL DAPT
[inch]
Total length
n.s.
CTL DAPT
[number]
Total branch points
**
CTL DAPT
[number/inch]
Relative branch point
*
CTL DAPT
[pixel/inch]
Mean width
**
CTL DAPT

A

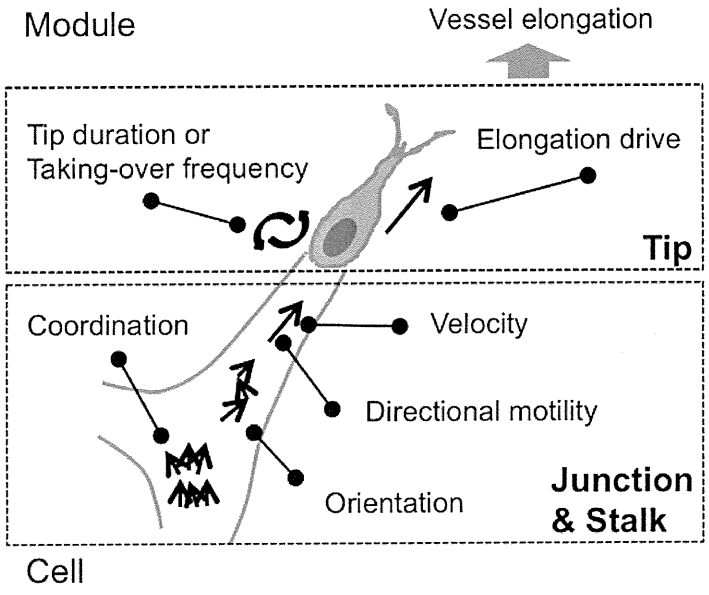

B

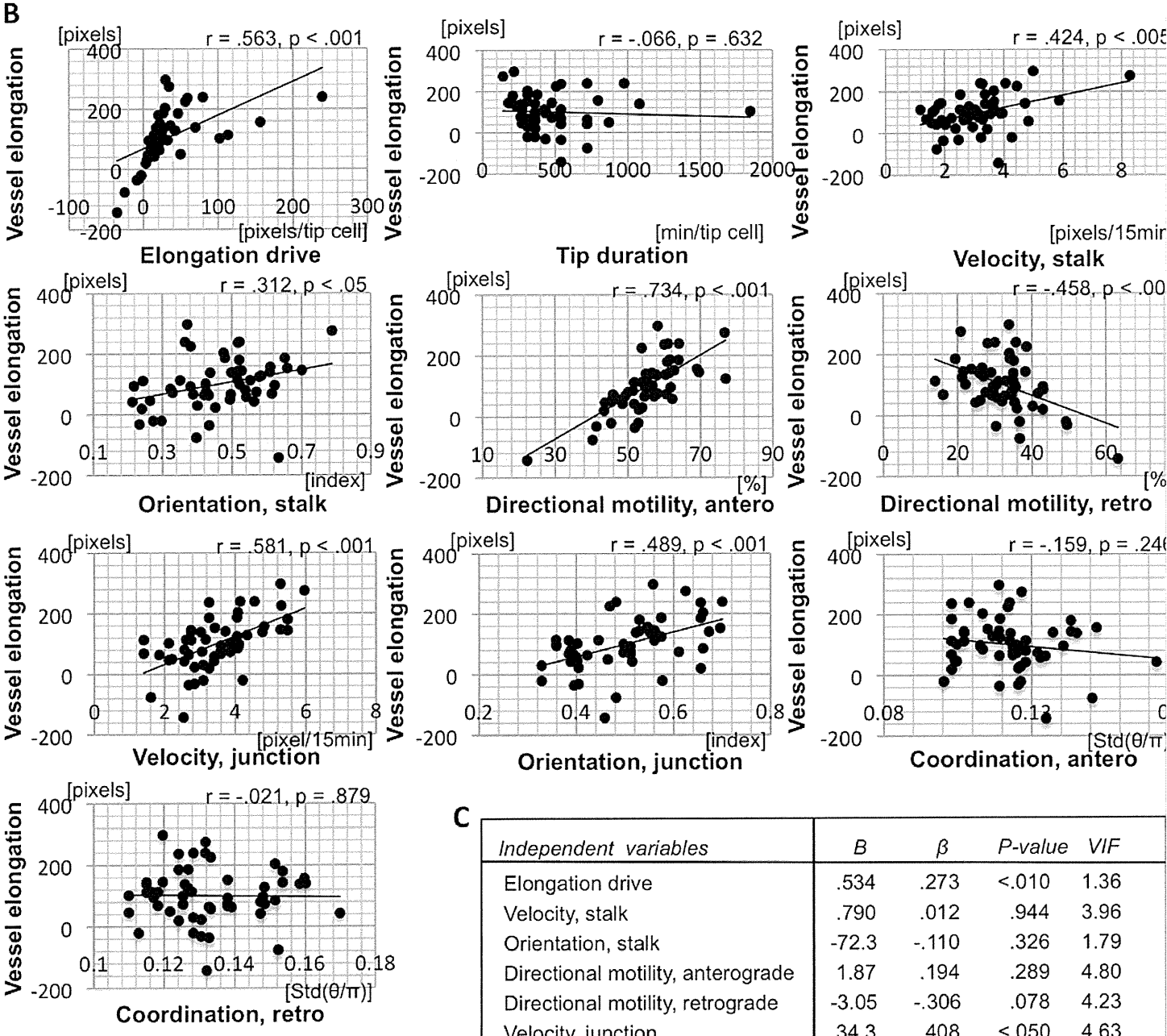

C

Independent variables	*B*	*β*	*P-value*	*VIF*
Elongation drive	.534	.273	<.010	1.36
Velocity, stalk	.790	.012	.944	3.96
Orientation, stalk	-72.3	-.110	.326	1.79
Directional motility, anterograde	1.87	.194	.289	4.80
Directional motility, retrograde	-3.05	-.306	.078	4.23
Velocity, junction	34.3	.408	<.050	4.63
Orientation, junction	88.9	.107	.280	1.42
adjusted R^2			.706	
F- value (P-value)			14.746 (0.000)	

Table S1. The percentage of ECs undergoing mitosis

	Tip*	Stalk**	Bridge†	Junction‡	Sheet§	All/n§	Ratio (%)
VEGF (0 ng/ml)	0	0	0	0	0	0/129	0.0
	0	2	0	0	8	10/233	4.3
	0	0	0	0	0	0/126	0.0
VEGF (5 ng/ml)	0	0	1	0	3	4/245	1.6
	0	0	0	1	1	2 /257	0.8
	0	1	3	4	1	9/217	4.1
VEGF (50 ng/ml)	0	3	2	0	0	5/83	6.0
	0	2	4	3	0	9/211	4.3
	0	0	0	1	1	2/178	1.1

The number of ECs undergoing mitosis at specified places.
*At the tip.
**At blunt-ended regions (including the tip) distal to the junctions.
†At regions connecting two junctions.
‡At regions where two or more stalks diverge or converge.
§At vascular beds where ECs form sheets.
§The total number of ECs observed.

Gene Expression Patterns 11 (2011) 371–377

Contents lists available at ScienceDirect

Gene Expression Patterns

journal homepage: www.elsevier.com/locate/gep

Identification and developmental analysis of endothelin receptor type-A expressing cells in the mouse kidney

Taro Kitazawa [1], Takahiro Sato [1,2], Koichi Nishiyama, Rieko Asai, Yuichiro Arima, Yasunobu Uchijima, Yukiko Kurihara, Hiroki Kurihara *

Department of Physiological Chemistry and Metabolism, Graduate School of Medicine, The University of Tokyo, 7-3-1 Hongo, Bunkyo-ku, Tokyo 113-0033, Japan

ARTICLE INFO

Article history:
Received 7 March 2011
Received in revised form 26 April 2011
Accepted 27 April 2011
Available online 1 May 2011

Keywords:
Endothelin receptor
Kidney
Metanephric mesenchyme
Smooth muscle cell
Juxtaglomerular cell

ABSTRACT

The endothelin (Edn) system plays pleiotropic roles in renal function and various disease processes through two distinct G protein-coupled receptors, Edn receptors type-A (Ednra) and type-B (Ednrb). However, difficulties in the accurate identification of receptor-expressing cells in situ have made it difficult to dissect their diverse action in renal (patho)physiology. We have recently established mouse lines in which *lacZ* and *EGFP* are 'knocked-in' to the *Ednra* locus to faithfully mark *Ednra*-expressing cells. Here we analyzed these mice for their expression in the kidney to characterize *Ednra*-expressing cells. *Ednra* expression was first observed in undifferentiated mesenchymal cells around the ureteric bud at E12.5. Thereafter, *Ednra* expression was widely observed in vascular smooth muscle cells, JG cells and mesenchymal cells in the interstitium. After growth, the expression became confined to vascular smooth muscle cells, pericytes and renin-producing JG cells. By contrast, most cells in the nephron and vascular endothelial cells did not express *Ednra*. These results indicate that *Ednra* expression may be linked with non-epithelial fate determination and differentiation of metanephric mesenchyme. *Ednra-lacZ/EGFP* knock-in mice may serve as a useful tool in studies on renal function and pathophysiology of various renal diseases.

Systemic and local circulatory homeostasis is maintained by a balance between vasoconstrictive and vasodilatory factors. The endothelin (Edn) system, composed of three peptide ligands (Edn1, Edn2 and Edn3) and their two G protein-coupled receptors (endothelin receptors type-A (Ednra) and type-B (Ednrb)), is involved in this mechanism (Masaki, 2004; Yanagisawa et al., 1988). In addition to their vasoconstrictive effects, Edns have a diverse set of biological activities such as proliferative effects on various cells, stimulation of hormone release and modulation of central nervous activity. During embryogenesis, the Edn1–Ednra axis regulates craniofacial and cardiovascular morphogenesis, whereas the Edn3–Ednrb axis contributes to melanocyte and enteric neuron development (Kurihara et al., 1999, 1994; Sato et al., 2008b).

The Edn system has been known to play pleiotropic roles in renal (patho)physiology. In the renal vasculature, Edn1 exerts potent vasoconstriction mainly through both Ednra (Hirata et al., 1989; Honing et al., 2000), whereas some vascular beds show an endothelium-dependent vasodilatory response mediated by Ednrb (Matsumura et al., 2000). Edn1 also acts on renal tubules to promote diuresis and natriuresis by several mechanisms via Ednrb (Ahn et al., 2004; Gariepy et al., 2000; Tomita et al., 1993). Furthermore, Edn1 modulates renin secretion from juxtaglomerular (JG) cells (Rakugi et al., 1988). Through these effects, the Edn system has been implicated in the pathophysiology of hypertension and various renal diseases.

To dissect mechanisms underlying these diverse roles of the Edn system, identification of cells expressing the Edn receptors is of fundamental importance. However, accurate description of their expression patterns remains still elusive due to relatively low expression levels and lack of antibodies sufficient for immunostaining. We have recently established mouse lines in which marker genes such as *lacZ* and *EGFP* are 'knocked-in' to the *Ednra* locus (Asai et al., 2010; Sato et al., 2008a). In these mice, the marker gene expression faithfully recapitulates that of the endogenous *Ednra* during embryogenesis. In this study, we analyzed these mice for renal expression to clarify the localization of Ednra and its developmental changes in the kidney.

1. Results

1.1. Isolation of Ednra–EGFP-positive cells and gene expression profiling by RT-PCR

In *Ednra-lacZ* or *-EGFP* knock-in mice, marker gene expression patterns faithfully recapitulate those of endogenous *Ednra*

* Corresponding author. Tel.: +81 3 5841 3498; fax: +81 3 5684 4958.
E-mail address: kuri-tky@umin.ac.jp (H. Kurihara).
[1] These authors contributed equally to this study.
[2] Present address: Yamanaka iPS Cell Special Project, Japan Science and Technology Agency, Kawaguchi 332-0012, Japan.

1567-133X/$ - see front matter © 2011 Elsevier B.V. All rights reserved.
doi:10.1016/j.gep.2011.04.001

expression in the heart and pharyngeal arches (Asai et al., 2010; Sato et al., 2008a). To confirm that *Ednra-lacZ/EGFP* expression also reflects endogenous *Ednra* expression in the kidney, we performed FACS and RT-PCR. Cells were isolated from the E17.5 *Ednra*$^{EGFP/+}$ kidneys and subjected to forward-side selection to preliminarily identify cells (Fig. 1A), FACS analysis using fluorescent lectin revealed that endothelial cells (detected by BS-1), proximal tubules (detected by LTA) and collecting ducts (detected by DBA) were sufficiently collected (Fig. S1), indicating that overall cell populations of the kidneys were properly obtained through our manipulation. After PI-selection to exclude non-viable cells (Fig. 1B), EGFP-positive and -negative cells were sorted for RT-PCR analysis (Fig. 1C). *Ednra*-expressing cells were detected only in the EGFP-positive fraction, while *Ednrb* expression was detectable only in the EGFP-negative fraction (Fig. 1D). This result indicates that the knocked-in EGFP expression appears to faithfully recapitulate endogenous *Ednra* expression and there is little overlapping in the expression of *Ednra* and *Ednrb* in the developing kidney. *Platelet-endothelial cell adhesion molecule-1* (*PECAM1/CD31*; a marker for endothelial cells) and *α-smooth muscle actin* (*αSMA*; a marker for smooth muscle cells) expression was detected only in the EGFP-negative and -positive fractions, respectively (Fig. 1D). This finding coincides with the distinct expression pattern of Edn receptors in vasculature: *Ednra* and *Ednrb* in smooth muscle cells and endothelial cells, respectively (Masaki, 2004).

RT-PCR also revealed that *aquaporin-1* (*Aqp1*; a marker for proximal renal tubules) and *aquaporin-3* (*Aqp3*; a marker for collecting ducts) expression was undetectable in the EGFP-positive fractions (Fig. 1D). Instead, *glial cell line-derived neurotrophic factor* (*GDNF*; a marker for undifferentiated mesenchyme) and *renin-1* (*Ren1*; a marker for juxtaglomerular cells) expression was found only in the EGFP-positive fractions (Fig. 1D). These results indicate that *Ednra*-expressing cell population is likely to include vascular smooth muscle cells, JG cells and undifferentiated mesenchymal cells.

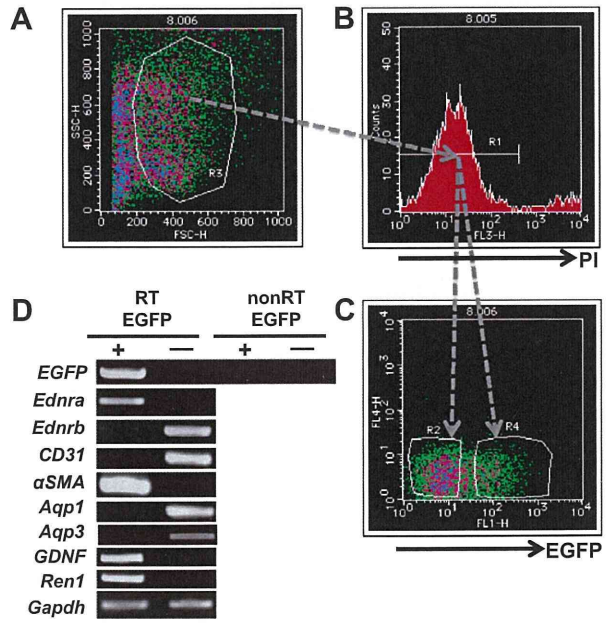

Fig. 1. Characterization of *Ednra-lacZ/EGFP*-expressing cells in the kidney. (A–C) Cells from the E17.5 *Ednra*$^{EGFP/+}$ embryonic kidneys were sorted into EGFP-positive and EGFP-negative fractions. Cells are subjected to forward-side selection for preliminary identification of the cells (A), next PI selection was performed to exclude nonviable cells (B), and finally EGFP selection was carried out to identify EGFP-expressing and EGFP-non-expressing cells (C). Gated R2 and R4 regions correspond to fractions of EGFP-negative and -positive cells, respectively. (D) RT-PCR analysis of EGFP-positive and -negative cells from the E17.5 kidneys. *Ednra* was detected only in the *Ednra–EGFP*-positive fraction. Expression of *Ednrb*, *CD31*, *αSMA*, *Aqp1*, *GDNF*, and *Ren1* was also analyzed. *Gapdh* was used as an internal control.

1.2. LacZ- and EGFP-labeling reveals the renal expression pattern of Ednra and its developmental changes

To analyze the expression pattern of *Ednra* in the kidney, we performed β-galactosidase staining on *Ednra-lacZ* knock-in embryonic and adult kidneys. *LacZ*-expressing cells were detected as early as E12.5 in mesenchyme around ureteric buds, although their expression levels were low compared to those in the lung and testis interstitium, where *Ednra* was most abundantly expressed at this stage (Fig. 2A and B). At E15.5 (Fig. 2C–E) and E18.5 (Fig. 2F–H), when basic expression patterns of *lacZ* are almost the same, *lacZ* expression was broadly distributed mainly in the medullary interstitial mesenchyme (Fig. 2C, D and F). By contrast, *lacZ* expression was relatively low in the cortical nephrogenic region (Fig. 2C, E and F). In higher magnification images, *lacZ*-expressing cells were detected in the vessel wall (Fig. 2G) and in the JG region encompassing intraglomerular mesangium and afferent and efferent arterioles (Fig. 2D–F). In adult sections, *lacZ* expression was apparently much sparser than in embryonic ones (compare Fig. 2I to C and F). At higher magnifications, *lacZ*-positive cells were observed around vessels (Fig. 2J) and in the JG region (Fig. 2K) as in embryonic sections. But, compared to developing kidneys, *lacZ*-positive cells were much decreased in the interstitium and inside the glomerulus. Throughout kidney development, renal tubular epithelium was not stained for β-galactosidase. These observations are consistent with the results of RT-PCR analysis described above.

To confirm that the *lacZ* expression patterns faithfully recapitulate the endogenous expression of *Ednra* in the kidney, we performed in situ hybridization on E18.5 kidney sections. *Ednra* expression was mainly distributed in the medullary interstitial region (Fig. S2A and B). High magnification images detected *Ednra* expression in the medullary interstitium (Fig. S2C and D), vessels (Fig. S2E) and the JG region (Fig. S2F). By contrast, renal tubules are apparently *LacZ*-negative (Fig. S2C–F). These patterns are largely identical to *Ednra-lacZ* expression patterns shown in Fig. 2.

To further dissect the characters of *Ednra*-expressing cells in the kidneys, we performed double immunostaining on *Ednra–EGFP* knock-in embryos and adult mice. We used CD31 and αSMA as markers for endothelial and smooth muscle cells, respectively. At E18.5, EGFP-expressing cells were detected around CD31-positive vascular endothelial cells and in the JG region (Fig. 3A–A‴). CD31-negative glomerular mesangial cells also showed EGFP expression (Fig. 3A–A‴). αSMA-positive cells are broadly observed along vessels and they are EGFP-positive (Fig. 3B–B‴). In the JG region, αSMA expression fades away as previously described (Sauter et al., 2008), and only EGFP signals remain (Fig. 3B–B‴). In addition, αSMA-negative and EGFP-positive cells were found in the interstitium (Fig. 3B–B‴).

In adult sections, EGFP signal was sparse, as seen in β-galactosidase staining. EGFP-expressing cells were detected in the vascular medial wall underlying CD31-positive endothelial cells (Fig. 3C–C‴) and in the JG region (Fig. 3D–D‴). Interestingly, EGFP expression in glomerular mesangial cells and the interstitium apparently was much less than in the developing kidney. To determine the character of *Ednra*-expressing cells in the interstitium, we observed some sections and checked approximately 1500 EGFP-positive cells, and found all the EGFP signals adjacent to CD31 signals (Fig. 3E–E‴), indicating that these *Ednra*-expressing cells are likely to be pericytes surrounding the descending vasa recta.

Taken these results together, *Ednra* expression in vascular smooth muscle cells and JG cells remain after birth, while

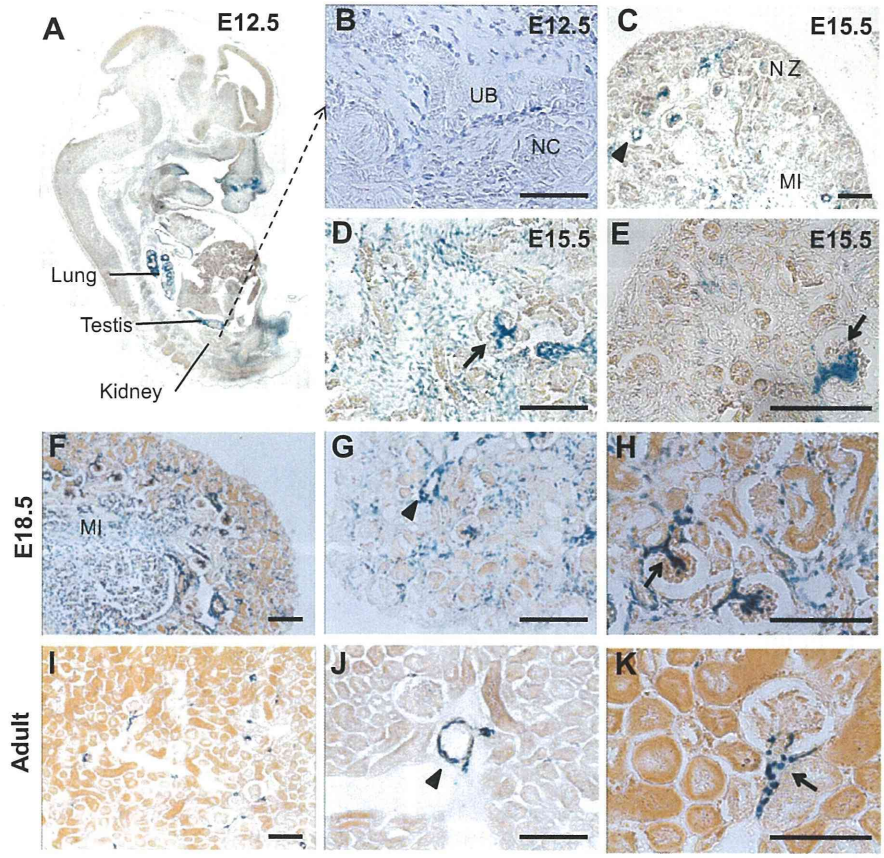

Fig. 2. β-Galactosidase staining in the *Ednra-lacZ* embryonic and adult kidneys. (A and B) A section of an E12.5 embryo stained for β-galactosidase activity. A is a low magnification image of the whole embryo and B is a high magnification image of the renal region of A. Renal *LacZ* signals can be detected but they are much weaker than those of the lung and testis. Signals are detected in mesenchyme around ureteric buds (UB), but not in nephrogenic condensates (NC). (C–E) Sections of the E15.5 kidneys stained for β-galactosidase activity. C is a low magnification image. (D and E) Higher magnification images of the medullary interstitial region and cortical nephrogenic region, respectively. (F–H) Low (F) and high (G and H) magnification images of E18.5 kidney sections stained for β-galactosidase activity. Basic expression pattern of *LacZ* in the E18.5 sections is the same with that of E15.5 ones. Abundant *LacZ* expression is detected throughout the medullary interstitium (C, D and F), but, compared with this, few signals can be detected in the nephrogenic mesenchyme of the cortical region (E). *LacZ* signal are detected around vessels (C, G, arrowheads) and the JG region including small vessels and intraglomerular mesangial cells (E, H, arrows). Renal tubules are apparently *LacZ*-negative. (I–K) Low (I) and high (J and K) magnification images of kidney sections of adult (2 months) mice stained for β-galactosidase activity. *LacZ*-expressing cells are detected around vessels (J, arrowhead) and in the JG region with adjacent small vessels (K, arrow), but are not detected in renal tubules as in embryonic sections. Compared to the developing kidney, *lacZ*-expressing cells were much decreased in the interstitium and inside the glomerulus (I). All the sections are counterstained with orange G. MI, medullary interstitium, NZ, nephrogenic zone. Scale bars: 100 μm.

expression in developing interstitial mesenchyme may be confined to pericytes.

1.3. Inclusion of renin-producing cells in Ednra–EGFP-positive cell population

Next we performed double immunostaining for EGFP and renin on *Ednra*$^{EGFP/+}$ kidney sections to confirm that renin-producing cells are Ednra-positive. At E18.5, renin-expressing cells were found not only in the JG region (Fig. 4A–A‴) but also in vessels outside the JG region (Fig. 4B–B‴) as previously described (Sauter et al., 2008). These renin-producing cells were always found to express EGFP (Fig. 4A–A‴ and B–B‴). In the adult kidneys, renin expression became restricted to cells within the JG region, which were also included within EGFP-positive cell population encompassing the afferent and efferent arterioles (Fig. 4C–C‴).

2. Discussion

In the present study, *Ednra*-positive cells in the kidney were clearly distinguished by marker gene expression. Renal *Ednra* expression was first observed in mesenchymal cells around the ureteric bud around E12.5. Thereafter, *Ednra* expression was broadly distributed in vascular smooth muscle cells, JG cells and mesenchymal cells in the interstitium until neonatal stages. After growth, the expression became confined to vascular smooth muscle cells, pericytes and renin-producing JG cells. By contrast, most cells in the nephron and vascular endothelial cells did not express *Ednra*. This pattern is quite distinct from that of *Ednrb*, which is abundantly expressed in tubular epithelial cells and vascular endothelial cells (Chow et al., 1995; Nangaku et al., 2002; Terada et al., 1992).

Kidney development initiates with the interaction between the Wolffian duct and metanephric mesenchyme (Vainio and Lin, 2002). The Wolffian duct generates the ureteric bud, which then invades the metanephric blastema to induce nephrogenic epithelial condensates destined to develop into nephrons. On the other hand, stromal cell progenitors that are not destined to nephrons are thought to become interstitial mesenchyme, vascular smooth muscle cells and JG cells (Humphreys et al., 2010; Kobayashi et al., 2008; Maric et al., 1997; Sequeira Lopez et al., 2004, 2001). Thus, *Ednra* expression may be linked with non-epithelial fate determination and differentiation of mesenchyme. This is in sharp

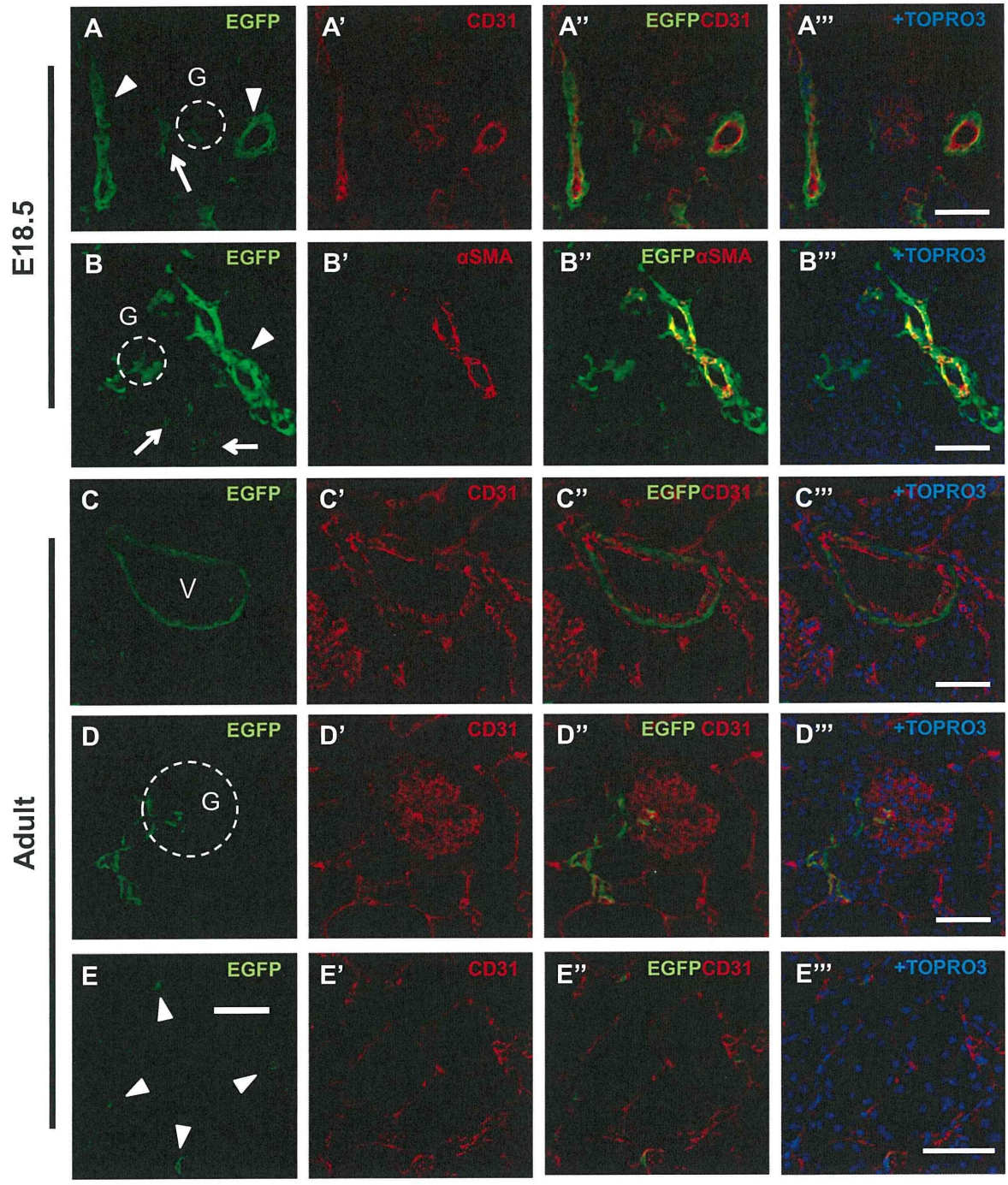

Fig. 3. Expression patterns of EGFP, CD31 and αSMA in *Ednra–EGFP* kidneys. Sections of E18.5 (A–A‴, B–B‴) and adult (C–C‴, D–D‴, E–E‴) kidneys immunostained for EGFP (A–E, A″–E″; green), CD31 (A′, A″, C′, C″, D′, D″, E′, E″; red), αSMA (B′, B″; red), and merged with TO-PRO-3 staining for nuclei (A‴–E‴; blue). In E18.5 kidneys, EGFP-positive cells are detected around CD31-positive vascular endothelial cells (A–A‴, arrowheads), and in the JG region (A–A‴, arrow). EGFP was co-expressed with αSMA in vessels (B–B‴, arrowhead), but not in the JG region (B–B‴, around glomerulus). EGFP-positive but αSMA-negative cells in the interstitium are indicated with arrows (B–B‴). In the adult kidneys, EGFP-positive cells are detected around CD31-positive endothelial cells (C–C‴) and in the JG region (D–D‴). Compared to the embryonic kidneys, EGFP signals are much decreased inside the glomerulus (D–D‴). EGFP-positive cells in the interstitium are associated with CD31-positive endothelial cells (E and E‴). G: glomerulus. Scale bars: 50 μm.

contrast to the expression of Ednrb, which is abundantly expressed in tubular epithelial cells that are derived from nephrogenic mesenchyme.

In addition to vascular smooth muscle cells, renin-producing JG cells shows intense staining for Ednra expression. This result is consistent with previous finding that Edn directly inhibit cAMP-dependent renin production through Ednra in cultured JG cells (Ryan et al., 2002). JG cells were postulated to derive from smooth muscle cells in the past (Owen et al., 1995). However, Sequeira Lopez et al. have shown that renin-producing precursor cells differentiate into a diversity of cells including smooth muscle cells (Sequeira Lopez et al., 2004, 2001). Furthermore, Matsushita

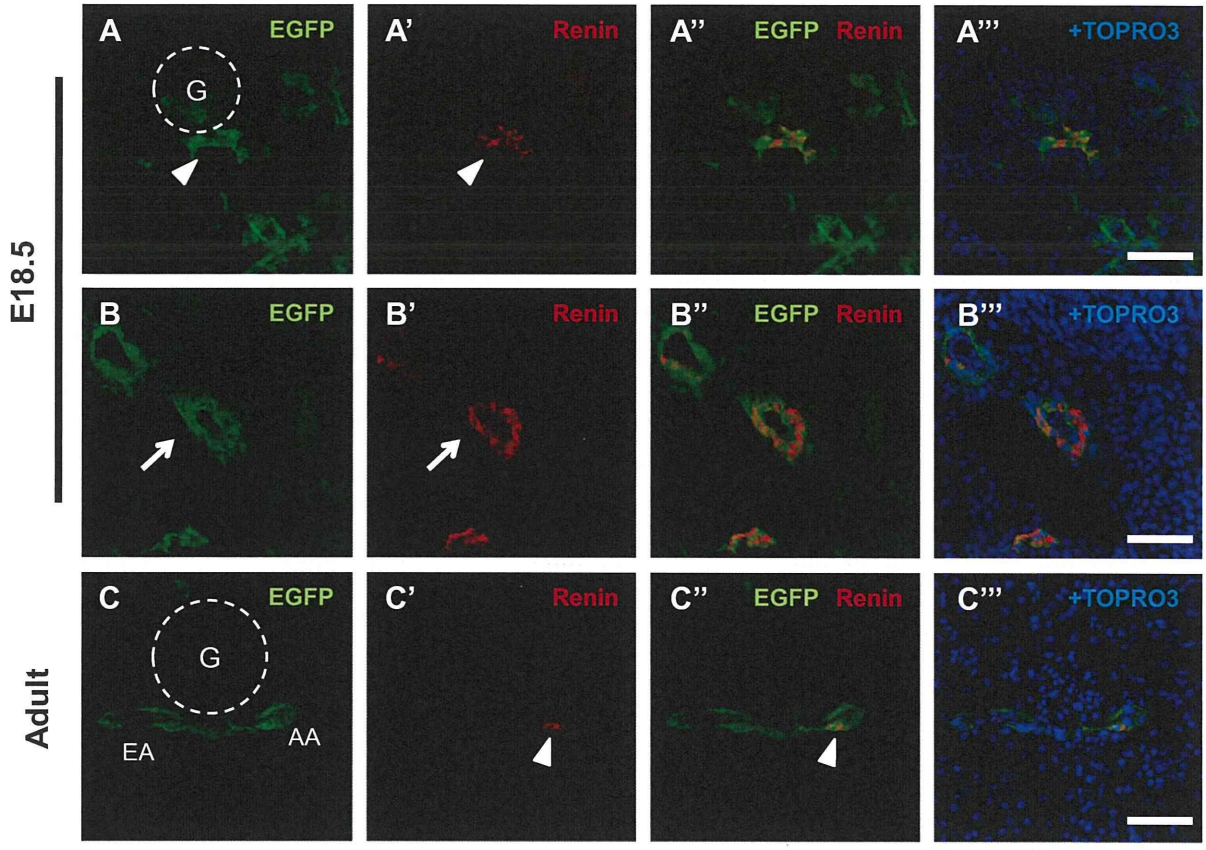

Fig. 4. Co-localization of EGFP and renin in *Ednra-EGFP* kidneys. Sections of kidneys of E18.5 (A–A″, B–B‴), and adult (C–C‴) mice, immunostained for EGFP (A–C, A″–C‴; green), renin (A′–C′, A″–C″; red), and merged with TO-PRO-3 staining for nuclei (A‴–C‴; blue). In both the E18.5 (A–A‴) and adult (C–C‴) JG region, rennin-producing cells are EGFP-positive (arrowheads). In E18.5 kidneys, rennin-producing cells are also detected in vessels outside the JG region, which are also EGFP-positive (arrows) (B–B‴). G: glomerulus. Scale bars: 50 μm.

et al. have demonstrated the presence of mesenchymal stem cells that may give rise to smooth muscle cells through renin-producing precursors (Matsushita et al., 2010). Although the origin of JG cells and their relationship to smooth muscle cells in the lineage hierarchy is still controversial, *Ednra* expression may serve as a hallmark for non-epithelialized metanephric descendants.

In the present study, *Ednra* expression appears to decrease in mesangium and interstitium after growth. On the other hand, Ednra has been implicated in various diseases involving these cell populations, such as glomerulonephritis and renal intestinal fibrosis (Brochu et al., 1999; Sorokin and Kohan, 2003). In these pathological conditions, *Ednra* expression may be re-activated in proliferative mesangial and/or mesenchymal cells, where Ednra may mediate a mitotic signal to contribute to disease progression.

It has been known that the Edn system is deeply involved in various renal (patho)physiology. However, dissection of its diverse action is difficult possibly because their different effects on the nephron and vasculature can hardly be discriminated (Dhaun et al., 2006). *Ednra*-knock-in mice may serve as a useful tool in such studies by enabling us to identify and isolate *Ednra*-expressing cells in various conditions.

3. Materials and methods

3.1. Mice

Ednra$^{lacZ/+}$ (*lacZ*-knock-in) and *Ednra*$^{EGFP/+}$ (*EGFP*-knock-in) mice, described previously (Asai et al., 2010; Sato et al., 2008a), were maintained on an ICR-background. Mice were housed in an environmentally controlled room at 23 ± 2 °C, with a relative humidity of 50–60% and under a 12L–12D light cycle. Genotypes were determined by PCR on tail-tip or amnion DNA using specific primers. Embryonic ages were determined by timed mating with the day of the plug being embryonic day (E) 0.5. All the animal experiments were reviewed and approved by the University of Tokyo Animal Care and Use Committee.

3.2. Cell sorting

Kidneys were collected from E17.5 *Ednra*$^{EGFP/+}$ and wild-type embryos and dissected into pieces. Then the kidneys were incubated in D-MEM (Wako) containing 1 mg/ml of collagenase (Sigma) at 37 °C for 60 min. After disaggregated in 0.05% trypsin–EDTA solution (Sigma) to obtain single-cell suspensions, cells were subjected to hypotonic treatment for hemolyzation and resuspended in an appropriate volume of FACS buffer (5% fetal bovine serum/PBS). For cell sorting, the cells were passed through a cell strainer (BD Bioscience) and sorted into EGFP-positive and EGFP-negative cells using a FACS VantageSE flow cytometer (BD Bioscience). The data were analyzed with CellQuest software (BD Bioscience). For FACS analysis, the cells collected form wild-type embryos were lectin stained. The cells were incubated with FITC-conjugated lectin from *Bandeiraea simplicifolia* (BS-1) (Sigma), FITC-conjugated *Dolichos biflorus* agglutinin (DBA) (J-Oilmills), or biotin-conjugated *Lotus tetragonolobus* agglutinin (LTA) (Vector) on ice for 30 min. The cells incubated with biotin-conjugated

LTA were washed with an excess amount of FACS buffer, and incubated with PE-conjugated streptavidin (BD Bioscience) on ice for 30 min. The cells were washed and resuspended in FACS buffer again at an appropriate concentration, and passed through a cell strainer before FACS analysis. Analyses were performed on a FACS VantageSE flow cytometer, and data were analyzed with CellQuest software. In the assay, electronic gating was set to exclude nonviable cells with propidium iodide (PI) (Sigma) staining after cellular fractionation on the basis of forward versus side scatter.

3.3. RT-PCR

After cell sorting, EGFP-positive and EGFP-negative cells were subjected to conventional RT-PCR. Extraction of total RNA, reverse-transcription, and conventional PCR was performed as described previously with minor modifications (Asai et al., 2010). PCR on the resulting cDNA was performed using the primers 5′-GACGTAAACGGCCACAAGTTCA-3′ and 5′-GAACTCCAGCAGGACCA TGTGATC-3′ for *EGFP* (product size, 608 bp: annealing temperature, 65 °C), 5′-ACGCTGGCCTTTCG-3′ and 5′-CTGAGCAGTTCACA CCGGTTCTTATC-3′ for *Ednra* (product size, 603 bp: annealing temperature, 62 °C), 5′-CACAGTGCTGAGTCTTTGTGCTCT-3′ and 5′-ACCTATGGGTTCGGGGACAG-3′ for *Ednrb* (product size, 157 bp: annealing temperature, 60 °C), 5′-AGGACAGACCCTTCCACCAA-3′ and 5′-AATGACAACCACCGCAATGA-3′ for *CD31* (product size, 206 bp; annealing temperature, 62 °C), 5′-TGCCGAGCGTGAGAT TG-3′ and 5′-AATGAAAGATGGCTGGAAGAGAG-3′ for *αSMA* (product size, 193 bp; annealing temperature, 62 °C), 5′-GGCTATGTG-CAGTGTCATGTC-3′ and 5′-CTGTGATATGCCAGTGGTCAG-3′ for *Aqp1* (product size, 462 bp; annealing, 62 °C), 5′-ATCAAG CTGCCCATCTACAC-3′ and 5′-GGGCCAGCTTCACATTCTC-3′ for *Aqp3* (product size, 559 bp; annealing temperature, 60 °C), 5′-CCAGA-GAATTCCAGAGGGAAAGGT-3′ and 5′-CAGATACATCCACACCG TTTAGCGG-3′ for *GDNF* (product size, 338 bp; annealing temperature, 60 °C), 5′-ATCCCGCTCAAGAAAATGCC-3′ and 5′-TGTGTCA CAGTGATTCCACC-3′ for *Ren1* (product size, 416 bp: annealing temperature, 62 °C), 5′-GGTGTGAACCACGAGAAATAT-3′ and 5′-AGAT-CCACGACGGACACATT-3′ for *Gapdh* (product seize, 334 bp: annealing temperature, 60 °C).

3.4. β-Galactosidase staining

lacZ expression was detected by staining with X-Gal (5-bromo-4-chloro-3-indolyl β-D-galactoside) for β-galactosidase activity. Section staining was performed as described previously with minor modifications (Nagy et al., 2003). Sections were counterstained with 1% orange G (Sigma).

3.5. In situ hybridization

Sections (12 μm) were prepared from frozen mouse kidney samples. Treatment for in situ hybridization was as described with minor modifications (Ishii et al., 1997). The *Ednra* probe has been described previously (Sato et al., 2008a).

3.6. Immunohistochemistry

Immunohistochemistry of sections was performed as described previously with minor modifications (Makita et al., 2008). Embryo cryosections (12 μm) were immunostained using the following antibodies: rat monoclonal anti-GFP (Nacalai Tesque, Kyoto, Japan; 1:200), rabbit anti-GFP (Medical and Biological Laboratories, Nagoya, Japan; 1:250), rat anti-CD31 (BD Pharmingen, 1:200), mouse anti-αSMA (Sigma, 1:500), goat anti-Renin (Santa Cruz, 1:100). Signals were visualized with Rhodamine Red- or FITC-conjugated secondary antibodies specific for the appropriate species. When visualizing signals with anti-mouse secondary antibody, we used M.O.M. Blocking Reagent (Vector) to reduce background staining. Nuclei were visualized with TO-PRO-3 (Molecular Probes).

Acknowledgements

We also thank Yuko Fujisawa and Sakura Kushiyama for technical assistance. This work was supported in part by Global COE Program (Integrative Life Science Based on the Study of Biosignaling Mechanisms), MEXT, Japan, grants-in-aid for scientific research from the Ministry of Education, Culture, Sports, Science and Technology, Japan, grants-in-aid for scientific research from the Ministry of Health, Labour and Welfare of Japan.

Appendix A. Supplementary data

Supplementary data associated with this article can be found, in the online version, at doi:10.1016/j.gep.2011.04.001.

References

Ahn, D., Ge, Y., Stricklett, P.K., Gill, P., Taylor, D., Hughes, A.K., Yanagisawa, M., Miller, L., Nelson, R.D., Kohan, D.E., 2004. Collecting duct-specific knockout of endothelin-1 causes hypertension and sodium retention. J. Clin. Invest. 114, 504–511.

Asai, R., Kurihara, Y., Fujisawa, K., Sato, T., Kawamura, Y., Kokubo, H., Tonami, K., Nishiyama, K., Uchijima, Y., Miyagawa-Tomita, S., et al., 2010. Endothelin receptor type A expression defines a distinct cardiac subdomain within the heart field and is later implicated in chamber myocardium formation. Development (Cambridge, England) 137, 3823–3833.

Brochu, E., Lacasse, S., Moreau, C., Lebel, M., Kingma, I., Grose, J.H., Lariviere, R., 1999. Endothelin ET(A) receptor blockade prevents the progression of renal failure and hypertension in uraemic rats. Nephrol. Dial. Transplant. 14, 1881–1888.

Chow, L.H., Subramanian, S., Nuovo, G.J., Miller, F., Nord, E.P., 1995. Endothelin receptor mRNA expression in renal medulla identified by in situ RT-PCR. Am. J. Physiol. 269, F449–457.

Dhaun, N., Goddard, J., Webb, D.J., 2006. The endothelin system and its antagonism in chronic kidney disease. J. Am. Soc. Nephrol. 17, 943–955.

Gariepy, C.E., Ohuchi, T., Williams, S.C., Richardson, J.A., Yanagisawa, M., 2000. Salt-sensitive hypertension in endothelin-B receptor-deficient rats. J. Clin. Invest. 105, 925–933.

Hirata, Y., Matsuoka, H., Kimura, K., Fukui, K., Hayakawa, H., Suzuki, E., Sugimoto, T., Yanagisawa, M., Masaki, T., 1989. Renal vasoconstriction by the endothelial cell-derived peptide endothelin in spontaneously hypertensive rats. Circ. Res. 65, 1370–1379.

Honing, M.L., Hijmering, M.L., Ballard, D.E., Yang, Y.P., Padley, R.J., Morrison, P.J., Rabelink, T.J., 2000. Selective ET(A) receptor antagonism with ABT-627 attenuates all renal effects of endothelin in humans. J. Am. Soc. Nephrol. 11, 1498–1504.

Humphreys, B.D., Lin, S.L., Kobayashi, A., Hudson, T.E., Nowlin, B.T., Bonventre, J.V., Valerius, M.T., McMahon, A.P., Duffield, J.S., 2010. Fate tracing reveals the pericyte and not epithelial origin of myofibroblasts in kidney fibrosis. Am. J. Pathol. 176, 85–97.

Ishii, Y., Fukuda, K., Saiga, H., Matsushita, S., Yasugi, S., 1997. Early specification of intestinal epithelium in the chicken embryo: a study on the localization and regulation of CdxA expression. Dev. Growth Differ. 39, 643–653.

Kobayashi, A., Valerius, M.T., Mugford, J.W., Carroll, T.J., Self, M., Oliver, G., McMahon, A.P., 2008. Six2 defines and regulates a multipotent self-renewing nephron progenitor population throughout mammalian kidney development. Cell Stem Cell 3, 169–181.

Kurihara, H., Kurihara, Y., Nagai, R., Yazaki, Y., 1999. Endothelin and neural crest development. Cell. Mol. Biol. (Noisy-le-grand) 45, 639–651.

Kurihara, Y., Kurihara, H., Suzuki, H., Kodama, T., Maemura, K., Nagai, R., Oda, H., Kuwaki, T., Cao, W.H., Kamada, N., et al., 1994. Elevated blood pressure and craniofacial abnormalities in mice deficient in endothelin-1. Nature 368, 703–710.

Makita, R., Uchijima, Y., Nishiyama, K., Amano, T., Chen, Q., Takeuchi, T., Mitani, A., Nagase, T., Yatomi, Y., Aburatani, H., et al., 2008. Multiple renal cysts, urinary concentration defects, and pulmonary emphysematous changes in mice lacking TAZ. Am. J. Physiol. Renal. Physiol. 294, F542–553.

Maric, C., Ryan, G.B., Alcorn, D., 1997. Embryonic and postnatal development of the rat renal interstitium. Anat. Embryol. (Berl) 195, 503–514.

Masaki, T., 2004. Historical review: endothelin. Trends Pharmacol. Sci. 25, 219–224.

Matsumura, Y., Kuro, T., Kobayashi, Y., Konishi, F., Takaoka, M., Wessale, J.L., Opgenorth, T.J., Gariepy, C.E., Yanagisawa, M., 2000. Exaggerated vascular and renal pathology in endothelin-B receptor-deficient rats with deoxycorticosterone acetate–salt hypertension. Circulation 102, 2765–2773.

Matsushita, K., Morello, F., Wu, Y., Zhang, L., Iwanaga, S., Pratt, R.E., Dzau, V.J., 2010. Mesenchymal stem cells differentiate into renin-producing juxtaglomerular (JG)-like cells under the control of liver X receptor-alpha. J. Biol. Chem. 285, 11974–11982.

Nagy, A., Gertsenstein, M., Vintersten, K., Behringer, R., 2003. Manipulating the Mouse Embryo: A Laboratory Manual, 3rd ed. Cold Spring Harbor Laboratory Press.

Nangaku, M., Yamada, K., Gariepy, C.E., Miyata, T., Inagi, R., Kurokawa, K., Yanagisawa, M., Fujita, T., Johnson, R.J., 2002. ET(B) receptor protects the tubulointerstitium in experimental thrombotic microangiopathy. Kidney Int. 62, 922–928.

Owen, R.A., Molon-Noblot, S., Hubert, M.F., Kindt, M.V., Keenan, K.P., Eydelloth, R.S., 1995. The morphology of juxtaglomerular cell hyperplasia and hypertrophy in normotensive rats and monkeys given an angiotensin II receptor antagonist. Toxicol. Pathol. 23, 606–619.

Rakugi, H., Nakamaru, M., Saito, H., Higaki, J., Ogihara, T., 1988. Endothelin inhibits renin release from isolated rat glomeruli. Biochem. Biophys. Res. Commun. 155, 1244–1247.

Ryan, M.J., Black, T.A., Millard, S.L., Gross, K.W., Hajduczok, G., 2002. Endothelin-1 increases calcium and attenuates renin gene expression in As4.1 cells. Am. J. Physiol. Heart Circ. Physiol. 283, H2458–2465.

Sato, T., Kawamura, Y., Asai, R., Amano, T., Uchijima, Y., Dettlaff-Swiercz, D.A., Offermanns, S., Kurihara, Y., Kurihara, H., 2008a. Recombinase-mediated cassette exchange reveals the selective use of Gq/G11-dependent and -independent endothelin 1/endothelin type A receptor signaling in pharyngeal arch development. Development (Cambridge, England) 135, 755–765.

Sato, T., Kurihara, Y., Asai, R., Kawamura, Y., Tonami, K., Uchijima, Y., Heude, E., Ekker, M., Levi, G., Kurihara, H., 2008b. An endothelin-1 switch specifies maxillomandibular identity. Proc. Natl. Acad. Sci. USA 105, 18806–18811.

Sauter, A., Machura, K., Neubauer, B., Kurtz, A., Wagner, C., 2008. Development of renin expression in the mouse kidney. Kidney Int. 73, 43–51.

Sequeira Lopez, M.L., Pentz, E.S., Nomasa, T., Smithies, O., Gomez, R.A., 2004. Renin cells are precursors for multiple cell types that switch to the renin phenotype when homeostasis is threatened. Dev. Cell 6, 719–728.

Sequeira Lopez, M.L., Pentz, E.S., Robert, B., Abrahamson, D.R., Gomez, R.A., 2001. Embryonic origin and lineage of juxtaglomerular cells. Am. J. Physiol. Renal. Physiol. 281, F345–356.

Sorokin, A., Kohan, D.E., 2003. Physiology and pathology of endothelin-1 in renal mesangium. Am. J. Physiol. Renal. Physiol. 285, F579–589.

Terada, Y., Tomita, K., Nonoguchi, H., Marumo, F., 1992. Different localization of two types of endothelin receptor mRNA in microdissected rat nephron segments using reverse transcription and polymerase chain reaction assay. J. Clin. Invest. 90, 107–112.

Tomita, K., Nonoguchi, H., Terada, Y., Marumo, F., 1993. Effects of ET-1 on water and chloride transport in cortical collecting ducts of the rat. Am. J. Physiol. 264, F690–696.

Vainio, S., Lin, Y., 2002. Coordinating early kidney development: lessons from gene targeting. Nat. Rev. Genet. 3, 533–543.

Yanagisawa, M., Kurihara, H., Kimura, S., Tomobe, Y., Kobayashi, M., Mitsui, Y., Yazaki, Y., Goto, K., Masaki, T., 1988. A novel potent vasoconstrictor peptide produced by vascular endothelial cells. Nature 332, 411–415.

Fig. S1

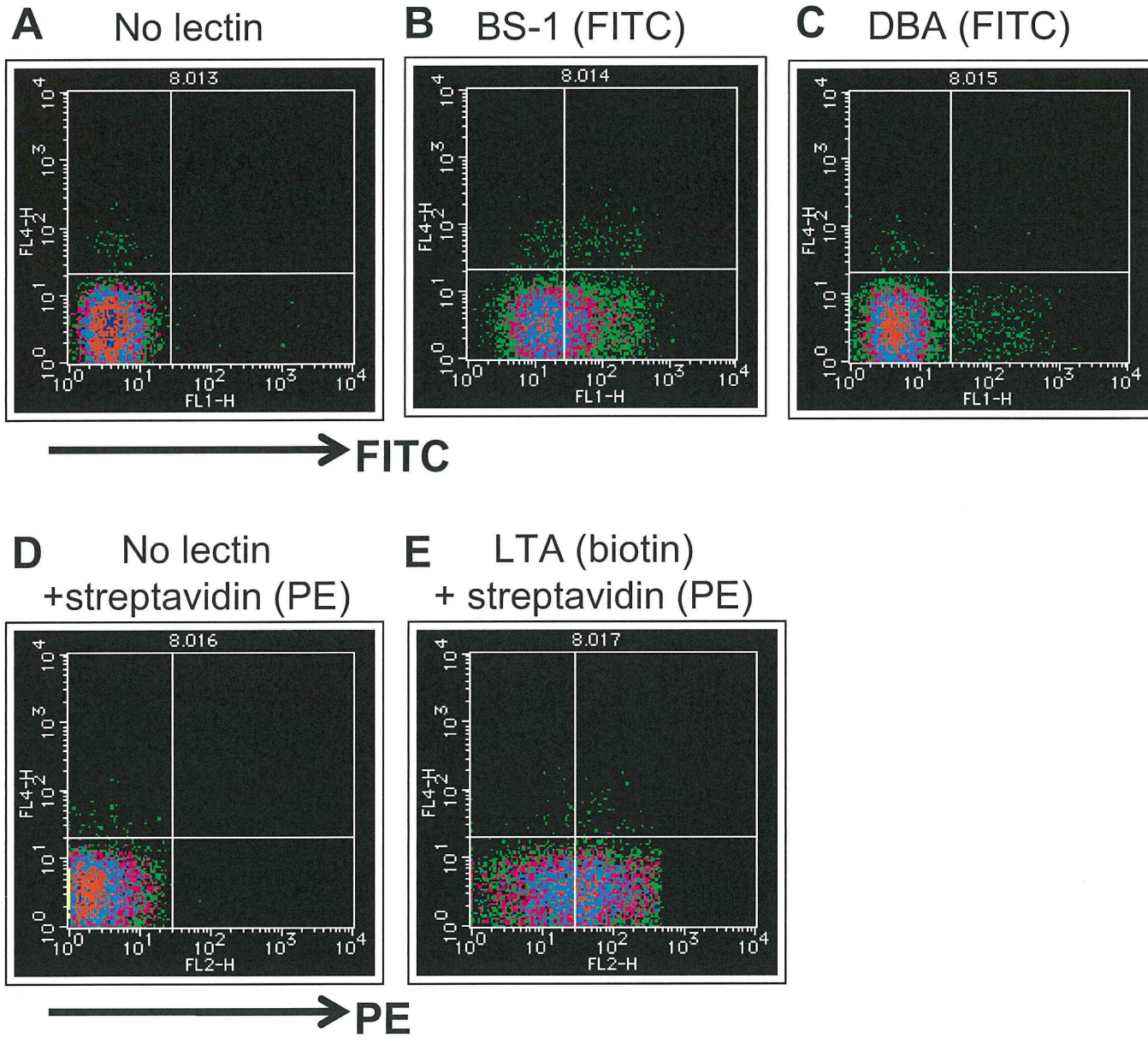
A No lectin
B BS-1 (FITC)
C DBA (FITC)
8.013
8.014
8.015
FL4-H
FL1-H
FITC
D No lectin
+streptavidin (PE)
E LTA (biotin)
+ streptavidin (PE)
8.016
8.017
FL2-H
PE

Fig. S2

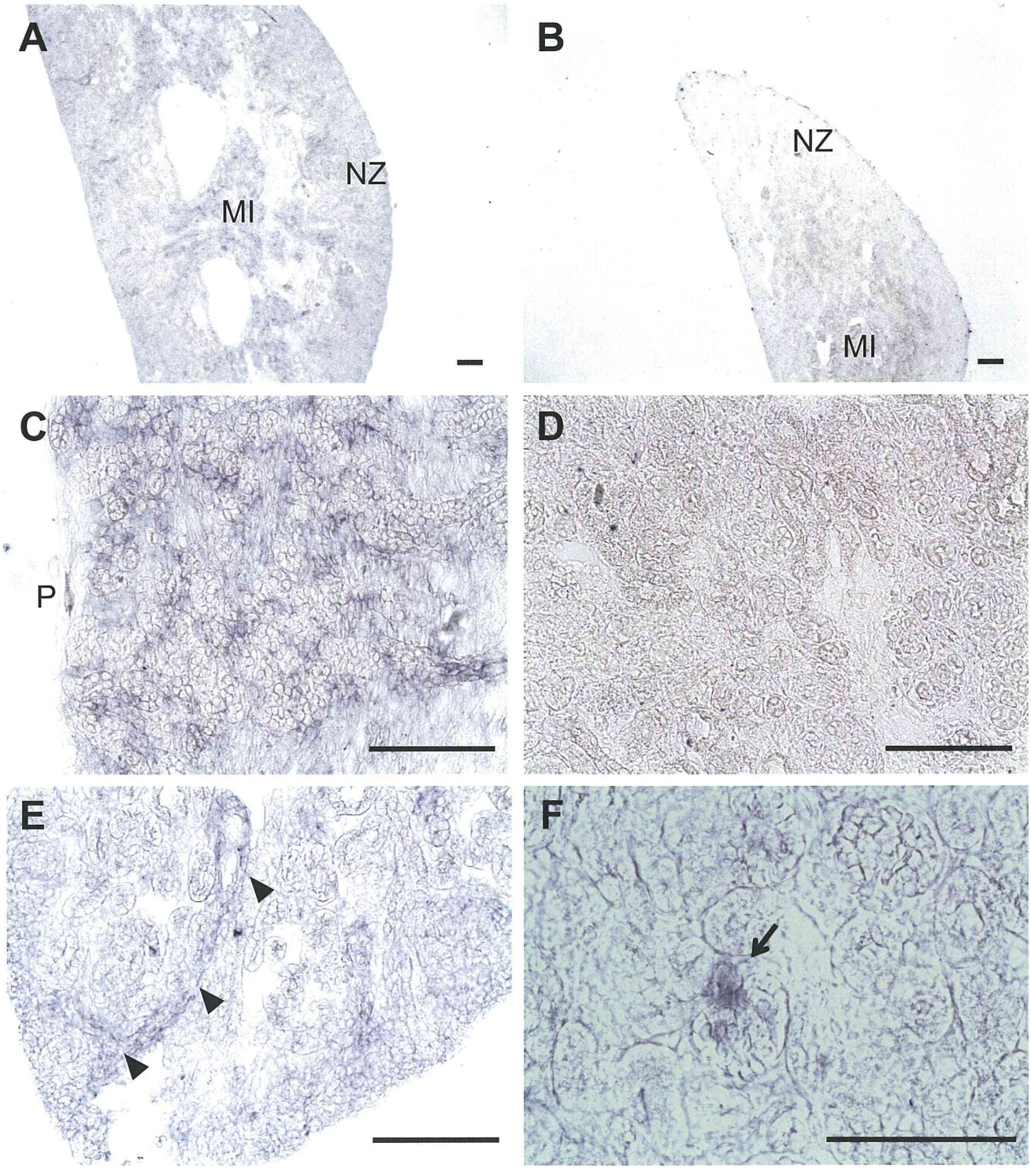

Calpain-6, a microtubule-stabilizing protein, regulates Rac1 activity and cell motility through interaction with GEF-H1

Kazuo Tonami[1,2], Yukiko Kurihara[1], Satoshi Arima[1], Koichi Nishiyama[1], Yasunobu Uchijima[1], Tomoichiro Asano[3], Hiroyuki Sorimachi[2] and Hiroki Kurihara[1,*]

[1]Department of Physiological Chemistry and Metabolism, Graduate School of Medicine, The University of Tokyo, 7-3-1 Hongo, Bunkyo-ku, Tokyo 113-0033, Japan
[2]Calpain Project, The Tokyo Metropolitan Institute of Medical Science (Rinshoken), 2-1-6 Kamikitazawa, Setagaya-ku, Tokyo 156-8506, Japan
[3]Department of Biomedical Chemistry, Hiroshima University Graduate School of Biomedical Sciences, Kasumi 1-2-3, Hiroshima 734-8551, Japan
*Author for correspondence (kuri-tky@umin.ac.jp)

Accepted 2 December 2010
Journal of Cell Science 124, 1214-1223

doi:10.1242/jcs.072561

Summary

Crosstalk between microtubules and actin filaments is crucial for various cellular functions, including cell migration, spreading and cytokinesis. The Rac1 GTPase plays a key role in such crosstalk at the leading edge of migrating cells in order to promote lamellipodial formation. However, the mechanism underlying the link between microtubules and Rac1 activation remains unclear. Here, we show that calpain-6 (CAPN6), a non-proteolytic calpain with microtubule-binding and -stabilizing activity, might participate in this crosstalk. Small interfering RNA (siRNA)-induced knockdown of *Capn6* in NIH 3T3 cells resulted in Rac1 activation, which promoted cell migration, spreading and lamellipodial protrusion. This increase in Rac1 activity was abolished by knockdown of the Rho guanine nucleotide exchange factor *GEF-H1* (officially known as *Arhgef2*). CAPN6 and GEF-H1 colocalized with microtubules and also interacted with each other through specific domains. Upon knockdown of *Capn6*, GEF-H1 was shown to translocate from microtubules to the lamellipodial region and to interact with Rac1. By contrast, RhoA activity was decreased upon knockdown of *Capn6*, although low levels of active RhoA or the presence of RhoA molecules appeared to be required for the *Capn6*-knockdown-induced Rac1 activation. We suggest that CAPN6 acts as a potential regulator of Rac1 activity, through a mechanism involving interaction with GEF-H1, to control lamellipodial formation and cell motility.

Key words: Actin, Calpain, Cell motility, Microtubule, Rac1

Introduction

Crosstalk between the two major cytoskeletal components, actin filaments and microtubules, is essential for various cellular functions, including cell migration, spreading and cytokinesis. In migrating cells, actin polymerization generates lamellipodial membrane protrusions at the leading edge, and actomyosin contractility in the tail promotes cell-body advancement (Chhabra and Higgs, 2007). In concert with the actin cytoskeleton, the dynamics of microtubules contributes to the establishment of cell polarity and the directional movement of migrating cells. The initial polarization of microtubule assembly is led by actin filaments, and conversely the polarized microtubules contribute to the reorganization of actin filaments (Li and Gundersen, 2008; Rodriguez et al., 2003; Siegrist and Doe, 2007).

Rho family GTPases and their regulatory proteins have been postulated to play central roles in microtubule–actin crosstalk. Microtubule depolymerization, by nocodazole or colchicine, induces Rho activation with an increase in stress fiber formation and cellular contractility (Enomoto, 1996; Ren et al., 1999). This effect is mediated by the Rho guanine-nucleotide-exchange factor GEF-H1 (officially known as ARHGEF2), which is released from microtubules upon depolymerization (Chang et al., 2008; Krendel et al., 2002). By contrast, microtubular growth after washout of nocodazole activates Rac1, leading to actin polymerization in lamellipodial protrusions (Waterman-Storer et al., 1999). Although GEF-H1 has been suggested as a potential mediator of microtubule–actin crosstalk at the leading edge (Siegrist and Doe, 2007; Waterman-Storer et al., 1999), this has not been proven. GEF-H1 was originally reported to be a GEF for both RhoA and Rac1 (Ren et al., 1998), but subsequent reports have not demonstrated a GEF activity for Rac1 (Benais-Pont et al., 2003; Glaven et al., 1999; Krendel et al., 2002; Zenke et al., 2004). Thus, the effect of GEF-H1 on Rac1 activity might depend upon the presence or absence of regulatory factors (Birkenfeld et al., 2008). A recent report has demonstrated that GEF-H1 can promote Rac1 activation in the presence of the p21-activated kinase PAK4 (Callow et al., 2005), indicating that the activation of Rac1 by GEF-H1 might be conditionally regulated.

The calpains are a family of intracellular cysteine proteases whose activity is highly dependent upon Ca^{2+} ions (Croall and Ersfeld, 2007; Goll et al., 2003; Hanna et al., 2008). Approximately one-half of calpains share a common four-domain structure comprising domains I to IV: domain II is a cysteine protease domain; domain III is related to the C2 domain, a Ca^{2+}- and phospholipid-binding module; and domain IV is characterized by the presence of multiple EF-hand motifs in some members, including the classical calpains (m- and μ-calpains) (Croall and Ersfeld, 2007; Goll et al., 2003). Among the 14 or 15 members of the calpain family in mammals, calpain-6 (CAPN6) is unique in that it lacks the active-site catalytic cysteine residue and is therefore